Journal of Materials Chemistry

Cite this: J. Mater. Chem., 2012, 22, 411

www.rsc.org/materials

PAPER

Direct growth of few-layer graphene films on SiO_2 substrates and their photovoltaic applications†

Hui Bi,[a] Shengrui Sun,[a] Fuqiang Huang,*[a] Xiaoming Xie[b] and Mianheng Jiang[b]

Received 26th September 2011, Accepted 5th October 2011
DOI: 10.1039/c1jm14778a

We first demonstrate the use of few layer graphene films directly grown on SiO_2 substrates obtained by ambient pressure chemical vapor deposition (APCVD) as counter electrodes in dye-sensitized solar cells (DSSCs). The layer number and crystal size of graphene films can be tuned by changing growth temperature, growth time and gas flow ratio (CH_4 : H_2). The continuous graphene films exhibit extremely excellent electrical transport properties with a sheet resistance of down to 63.0 Ω sq^{-1} and extremely high mobility of up to 201.4 cm^2 v^{-1} s^{-1}. The highly conductive graphene films as counter electrodes of DSSCs achieve a photovoltaic efficiency of 4.25%, which is comparable to the DSSC efficiency (4.32%) based on FTO counter electrodes. Our work indicates the great potential of CVD graphene films directly grown on dielectric substrates for photovoltaic and electronic applications.

1. Introduction

Graphene has recently attracted significant attention because of its unique optical and electrical properties.[1,2] Since the recent discovery of isolated graphene through mechanical exfoliation of bulk graphite,[1] chemical vapor deposition (CVD), among many developed methods, is widely applied to synthesize large-area graphene films on metal substrates (Cu, Ni, *etc.*).[3,4] Generally CVD-grown graphene requires transfer onto a desired substrate for further applications. Thus, it is necessary to directly prepare continuous graphene films on dielectric substrates (BN, Si, SiO_2, Al_2O_3, GaN, MgO, Si_3N_4, *etc.*). Considerable efforts have been made to directly grow graphene films on these substrates,[5–10] but so far the continuous and highly conductive films are hard to obtain.

The continuous and highly conductive graphene films are very useful for photovoltaic (PV) applications. Most of the CVD graphene films were transferred from those onto metal substrates. These graphene films have been employed as electrodes in organic photovoltaic cells (OPV),[11] Schottky solar cells[12] and CdTe solar cells[13] for the replacement of conventional transparent conductive films (TCFs), including In_2O_3:Sn (ITO), SnO_2:F (FTO), *etc.* However, the highest efficiency is only 4.17%,[13] which can still not compete with conventional solar cells. In addition, the graphene films not only need a complex wet-transfer process, which is unfavorable in current PV device fabrication, but also have relatively high sheet resistance (80–90% transparency). In practice, the high transmittance is not required for some electrode materials in thin-film solar cells (*e.g.* back electrodes). Therefore, it is desirable to develop a direct synthesis approach of highly conductive graphene films on dielectric substrates to replace the conventional TCFs for PV applications.

In this study, we report the direct growth of graphene films on the dielectric substrates by ambient pressure CVD (APCVD) at 1100–1200 °C. Layer number and crystal size of the graphene films are also tuned by varying growth conditions. The graphene films have outstanding electrical transport properties (sheet resistance: ~63.0 Ω sq^{-1}, electron mobility: ~201.4 cm^2 v^{-1} s^{-1}). The highly conductive films achieve a photovoltaic efficiency of 4.25% as counter electrodes in dye-sensitized solar cells (DSSCs).

2. Experimental

2.1 Graphene preparation

Dielectric substrates (SiO_2, Si, SiO_2/Si, AlN and BN) were used to grow graphene films using a gas mixture of methane (CH_4), hydrogen (H_2) and argon (Ar) by the APCVD method. Firstly, the substrates (1.0 × 1.0 cm^2) were washed in isopropanol and acetone for 10 min, then rinsed with deionized water and dried for use. Sequently, the substrates were placed in the center of a horizontal Al_2O_3 tube mounted inside a high-temperature furnace, then heated to reaction temperature (1100–1200 °C) under the flow of Ar and H_2. Finally, CH_4 was introduced in the chamber, and the specific flow rates of CH_4, H_2, and Ar were

[a]*State Key Laboratory of High Performance Ceramics and Superfine Microstructure and CAS Key Laboratory of Materials for Energy Conversion, Shanghai Institute of Ceramics, Chinese Academy of Sciences, Shanghai, 200050, China. E-mail: huangfq@mail.sic.ac.cn; Fax: +86 21 52416360; Tel: +86 21 52411620*
[b]*State Key Laboratory of Functional Materials for Informatics, Shanghai Institute of Microsystem and Information Technology, Chinese Academy of Sciences, Shanghai, 200050, China*

† Electronic supplementary information (ESI) available: growth conditions and preparation profile of CVD graphene films, SEM images, Raman spectra, AFM image. See DOI: 10.1039/c1jm14778a

adjusted to grow the graphene films for different time periods. After the graphene growth, the CH_4 gas flow was shut down, and the samples were cooled down to 500 °C at a rate of 10 °C min^{-1} under the same flow rates of H_2 and Ar as the growth stage. Detailed experimental conditions are listed in Table S1, and the preparation profile is shown in Figure S1.†

2.2 Fabrication of dye-sensitized solar cells

Firstly, 12 μm thick transparent films of commercial 20 nm sized TiO_2 particles (P25) were coated on FTO/glass substrates by using the doctor blade technique. The electrodes were sintered in dry air at 450 °C for 30 min. Subsequently, the electrodes were immersed in a 0.3 mM solution of ruthenium dye N719 in anhydrous ethanol overnight. Furthermore, Pt sputtered onto FTO/glass and graphene films/SiO_2 substrates were used as the counter electrodes. The electrolyte used consisted of 0.1 M LiI, 0.05 M I_2, 0.3 M 1,2-dimethyl-3-propylimidazolium iodine, and 0.5 M *tert*-butylpyridine in 3-methoxypropionitrile. Finally, the photoanode and the counter electrode were assembled and clipped in a sandwich type arrangement with the electrolyte solution placed in between.

2.3 Characterization and measurement

The morphology of graphene films on SiO_2 substrates was investigated by a Hitachi S-4800 field emission scanning electron microscope (FESEM) operated at 1 kV. The optical transmittance characteristics were determined *via* UV-vis diffuse reflectance spectrum in a spectrophotometer (Hitachi U-4100). High resolution transmission electron microscopy (HRTEM) images and selected area electron diffraction (SAED) patterns of graphene sheets, which were scraped from the surface of SiO_2 substrates, were performed on a JEOL JEM 2100F transmission electron microscope with an accelerating voltage of 200 kV. Raman spectra of the graphene films on dielectric substrates were obtained with Raman spectroscopy having a laser excitation energy of 532 nm. The electrical transport properties of graphene films were measured by the Van der Pauw method with an Accent HL5500. Photocurrent density–voltage characteristics (*J–V*) were measured using a Keithley Model 2440 source meter under AM 1.5 illumination. A 1000 W Oriel solar simulator was used as a light source and the power of the light was calibrated to one sun light intensity by using a NREL-calibrated Si cell (Oriel 91150).

3. Results and discussion

The direct growth of graphene TCFs on SiO_2 substrates can be carried out by the APCVD method in the growth temperature range of 1100–1200 °C, and the layer number of the continuous graphene films can be optimized to 2 for the samples S1 (growth temperature: 1200 °C, Ar : H_2 : CH_4 = 450 : 50 : 7 in sccm and growth time: 60 min), S2 (growth temperature: 1150 °C, Ar : H_2 : CH_4 = 450 : 10 : 3 in sccm and growth time: 120 min) and S3 (growth temperature: 1100 °C, Ar : H_2 : CH_4 = 450 : 30 : 10 in sccm and growth time: 120 min). Further experimental conditions are described in the ESI.†

Fig. 1a shows Raman spectra of the graphene films directly grown on SiO_2 substrates, including D (1351 cm^{-1}), G (1591 cm^{-1}) and 2D (2684 cm^{-1}) bands, which are the main

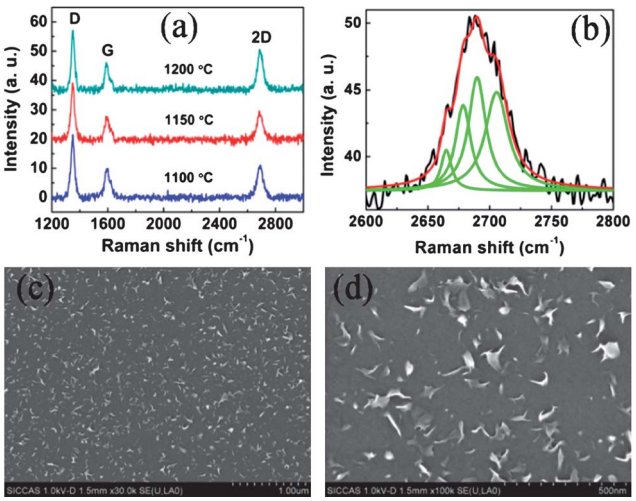

Fig. 1 (a) Raman spectra of the graphene films directly on SiO_2 substrates at 1100 °C, 1150 °C and 1200 °C, respectively. (b) Raman 2D peak fittings with four *Lorentz* peaks and (c, d) low- and high-magnification FESEM images of the graphene film (sample S1).

hallmarks of graphene.[14] The 2D band shows nearly the same intensity as the G band with 2D : G intensity ratios of ~1.2. The full width at half-maximum (FWHM) of the 2D band is ~50 cm^{-1}, exceeding the FWHM of ~30 cm^{-1} for single-layer graphene.[14] Furthermore, the 2D band can be fitted with four *Lorentzian* peaks (Fig. 1b), rather than a single *Lorentzian* peak.[14] The above features suggest that our graphene films for the samples S1, S2 and S3 have a typical bilayer structure, which can be further confirmed by AFM observation (Figure S2).† Moreover, Raman spectra from over 100 points were carried out, as shown in Figure S3, suggesting good uniformity of the graphene films.

The uniformity of the graphene films can be evaluated *via* FESEM images, as shown in Fig. 1c, 1d and S4.† It can be found that the entire SiO_2 surface is fully covered by a continuous graphene film, the surface of the graphene films are not smooth or flat, and some graphene sheets with the sizes of 50–100 nm are vertically grown and randomly oriented on the substrate surface to form three-dimensional (3D) structure, which is definitely different from those of FTO, ITO and graphene TCFs grown on the transition metals (Ni, Cu, *etc.*).[3,4] The unique 3D structure could make the graphene films possess a larger surface area, which is beneficial for forming conductive networks with semiconductor materials for the effective collection of electrons/holes in PV devices.[15]

A series of systematic experiments were carried out to study the dependence of growth time on the morphology and microstructure of graphene films. Raman spectra of graphene films on SiO_2 substrates with the gas flow rate of Ar : H_2 : CH_4 = 450 : 50 : 7 sccm for 60 min (sample S1), 90 min (sample S4) and 120 min (sample S5) growth at 1200 °C were obtained, as shown in Fig. 2a. For the samples S1, S4 and S5, the G bands are blue-shifted to 1591 cm^{-1}, compared with that (1580 cm^{-1}) for graphitic carbon materials, which is attributed to the presence of nanocrystalline graphite.[5] The presence of D bands, as shown in Fig. 2a, is due to not only the high fraction of the open edge of small-size graphene sheets, but also the defects inside graphene

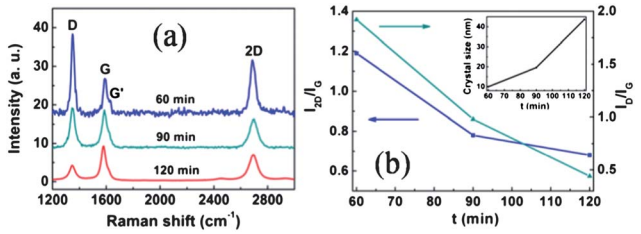

Fig. 2 (a) Raman spectra and (b) the intensity ratios $I_{2D} : I_G$ and $I_D : I_G$ of graphene films on SiO_2 substrates as a function of growth time at 1200 °C, inset of Figure 2b shows the calculated in-plane crystal size as a function of growth time.

sheets. Besides, the D′ band at 1620 cm^{-1} is another piece of evidence that the graphene films consist of quite a few small-size graphene sheets with some inter-crystalline defects.[16]

In order to quantitatively estimate the crystalline structure of graphene films, the ratios of the D : G intensity ($I_D : I_G$) and the 2D : G intensity ($I_{2D} : I_G$) of graphene films were contracted, as shown in Fig. 2b. With the increase in the growth time from 60 min to 120 min, the intensity ratio $I_{2D} : I_G$ decreases from 1.19 to 0.68, indicating the increase in the number of graphene layers. In addition, the intensity ratio $I_D : I_G$ decreases from 1.92 to 0.44. The reducing $I_D : I_G$ indicates decreasing defects inside graphene sheets. The intensity ratio ($I_D : I_G$) is directly related to the in-plane crystallite size (L_a), which can be calculated using the relation of $L_a = (2.4 \times 10^{-10}) \cdot \lambda^4 \cdot (I_D : I_G)^{-1}$, where I_D and I_G are the intensities of the D and G bands, respectively, and λ^4 is the wavelength of the laser.[17] The calculated crystallite sizes are plotted as a function of growth time in the inset of Fig. 2b. The crystalline size of the graphene film for the 60 min growth at 1200 °C is about 10.0 nm, and the crystalline size increases to 43.7 nm, when the growth time increases to 120 min.

In order to determine the layer number and crystal structure of the graphene films for different growth time, HRTEM images and SAED patterns were obtained in Fig. 3. It is apparent that by varying the growth time from 60 to 120 min, layer numbers of our graphene films are tunable in the range of 1–10, and the crystal structure of graphene films can be controlled. For the 60 min growth, a HRTEM image and the corresponding SAED pattern of the graphene film are shown in Fig. 3a & 3d. Based on the TEM observation, the edges of the graphene film are curved instead of straight (graphene films grown on Ni or Cu substrates), the layer number is very difficult to determine due to small-size graphene sheets (~10 nm), and it can be confirmed with Raman spectra that the graphene film is a 1–3 layer structure. Moreover, the ambiguous diffraction ring pattern further confirms that the film is typically a disordered structure, and the crystallinity degree of the graphene film is very low. In case of the 90 min growth, it is clear that the graphene sheets grow larger, their layer numbers (3–5 L) are very easy to obtain by observing the edges of the graphene sheets (Fig. 3b), and the calculated interlayer spacing is about 3.40 Å. Electron diffraction on the graphene film (Fig. 3e) reveals that the crystalline structure becomes more regular. When the growth time increases to 120 min, obvious parallel edges of the graphene film are observed, the graphene sheets are typically 7–10 graphitic layers (Fig. 3c), and their crystalline can be further improved (Fig. 3f). The above observation and analysis reveals that the graphene sheets not only grow thicker, but also grow larger in a lateral direction with the increase in growth time.

In order to study the morphology evolution of graphene growth on SiO_2 substrates, SEM images of graphene growth were obtained by varying the growth time to 10–120 min at 1200 °C with the Ar : H_2 : CH_4 flow rates equal to 450 : 50 : 7, as shown in Fig. 4. At the initial stage (10 min), some graphene islands with single- or bilayer structure could randomly form on SiO_2 substrate surface (Fig. 4a). As the growth proceeded, the graphene islands grew larger and larger in the lateral direction, and more graphene islands simultaneously formed on the substrate surface (Fig. 4b). When the growth time reached 30 min, a large amount of small-size graphene sheets were formed to achieve nearly full coverage on the SiO_2 substrates (Fig. 4c). With the increase in growth time to 60 min, some vertical graphene sheets randomly grew on the substrate surface due to the presence of the high energy graphene edge (Fig. 4d). When the growth time further increased to 90 and 120 min, the high-density graphene sheets (~50–100 nm in size) formed with a network structure (Fig. 4e & 4f), and the graphene sheets grew thicker from bilayers to a few layers (~10 L). The experimental study of the nucleation and growth dynamics complemented by different growth stages makes it possible to establish clear correlations

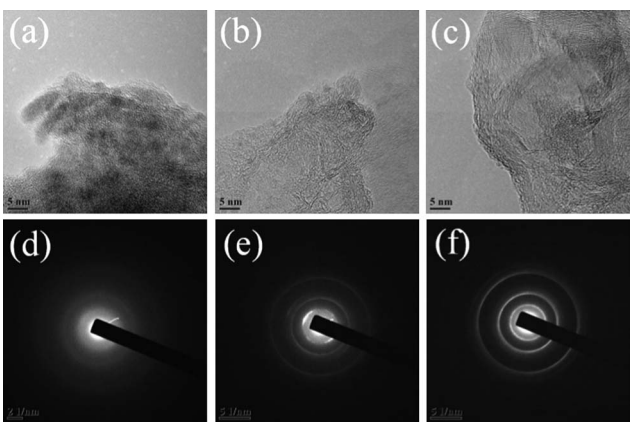

Fig. 3 (a–c) TEM images and (d–f) corresponding SAED patterns of graphene films directly grown on the SiO_2 substrates for 60 min, 90 min and 120 min growth at 1200 °C.

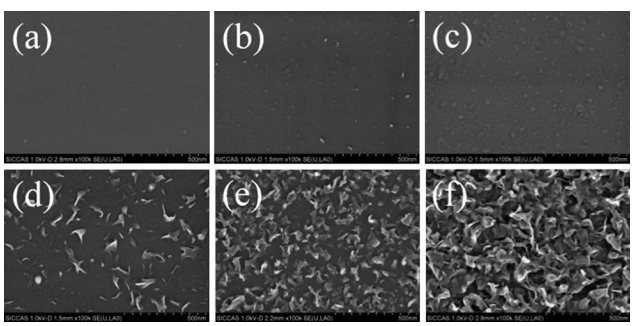

Fig. 4 SEM images of graphene films directly grown on SiO_2 substrates for the growth time of 10 min, 20 min, 30 min, 60 min, 90 min and 120 min, respectively, at 1200 °C.

between the growth parameters and the morphological features of graphene films. This also offers the possibility to precisely tailor the structure and morphologies of the catalyst-free graphene films.

In addition, the effect of the flow rate ratio of CH_4 to H_2 and growth substrates on the graphene growth was also investigated. The study shows that a high flow rate ratio of CH_4 to H_2 not only favors the formation of thicker graphene sheets, but also can form larger graphene sheets in the lateral direction with few defects (Figure S5).† Moreover, it needs to be noted that the graphene film growth is not strongly dependent on growth substrates. Without any metallic catalyst, graphene films could directly grow on BN, Si, AlN and SiO_2/Si substrates using the same growth conditions as the graphene films grew on the SiO_2 substrates, as shown in Fig. 5. Similar morphologies, microstructure and electrical properties of graphene films were achieved by varying growth conditions. This will open up a possibility for the direct fabrication of FET devices on graphene films without any transfer process.

The graphene films directly grown on SiO_2 substrates possess outstanding optical and electrical characteristics. Optical images of the graphene/SiO_2 transparent electrodes grown at 1200 °C for 30, 60, 90 and 120 min at ambient pressure are shown in Fig. 6a. It is clear that graphene simultaneously grows on both sides of the SiO_2 substrates, and each side nearly has the same sheet resistance. Thus, the single side transmittances of the graphene films grown on the SiO_2 substrates were extracted from the measured transmittance according to the equation of $T = T_m^{1/2}$, where T is the calculated single side transmittance of graphene films, and T_m is the measured transmittance. Their optical transparencies and sheet resistances are provided in Fig. 6b & 6c and Table 1. It is apparent that both sheet resistance and visible-infrared transparency decrease with increasing thickness of graphene films due to the increase in growth time. Particularly, the graphene films for the 30 and 60 min growth exhibit high transparencies of 98.1% and 94.0% at a 550 nm wavelength, and the corresponding average sheet resistances are 16540 Ω sq^{-1} and 4250 Ω sq^{-1}. Their transparencies are much superior to other conventional TCF's especially at long wavelengths.[18–20] However, at a similar transparency, the electrical properties are inferior to those of the CVD graphene grown with a Ni and Cu metal catalyst on SiO_2/Si,[3,21] but are much better than that of the

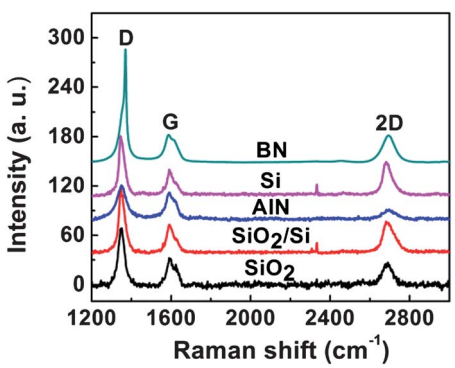

Fig. 5 Raman spectra of graphene films directly grown on different substrates at 1200 °C (Ar : H_2 : CH_4 = 450 : 50 : 7 in sccm) for 60 min growth.

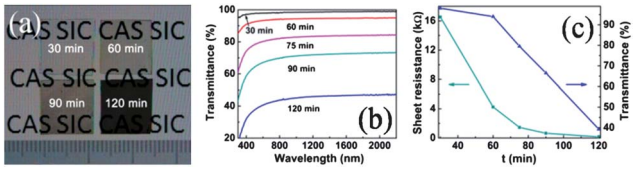

Fig. 6 (a) Optical images of graphene directly grown on SiO_2 substrates at 1200 °C for the growth time of 30 min, 60 min, 90 min and 120 min, respectively. (b) Optical transmittance spectra of the transferred graphene films. (c) Transmittance (at 550 nm) and sheet resistance as a function of growth time.

800 °C annealed films (8 kΩ sq^{-1}, 80% transparency) fabricated from graphene oxide[22] and graphene films (4–20 kΩ sq^{-1}, 80–90% transparency) directly grown on SiO_2 substrates by PECVD and LPCVD methods.[6,8] By further prolonging growth duration, their transmittances decrease rapidly to 79.5%, 66.9% and 39.6% at a 550 nm wavelength for 75 min, 90 min and 120 min growth, respectively, and respective sheet resistances are 1449 Ω sq^{-1}, 659 Ω sq^{-1} and 158 Ω sq^{-1}, respectively, indicating that the graphene TCFs have potential applications in future transparent and conductive electronics.

Moreover, the sheet resistance of graphene films can be further reduced to 63.0 Ω sq^{-1} by increasing the growth time and the CH_4 flow rate for samples S12 and S13, and the corresponding electron mobility reaches up to 201.4 cm^2 v^{-1} s^{-1}. Therefore, such low sheet resistances and high electron mobilities of graphene films used as electrode materials may allow light-induced electrons to be more promptly collected for the efficiency improvement of PV devices.

To demonstrate the applications of graphene films directly grown on SiO_2 substrates in thin film solar cells, a DSSC prototype device was fabricated, which contains a graphene/Pt counter electrode, a dye-sensitized porous TiO_2 photoanode and electrolyte between the two electrodes, as shown in Fig. 7a. A reference sample was prepared by using a FTO/Pt counter electrode, and this choice is partially based on the consideration

Table 1 Transmittance (T_{r550}) at a 550 nm wavelength, sheet resistance (R_s), and electron mobility (μ) of various graphene films (GFs) and FTO[a]

TCF	$T_{r\ 550}$ (%)	R_s (Ω sq^{-1})	μ (cm^2 v^{-1} s^{-1})
GF_{30min}	98.1	16540	35.8
GF_{60min}	94.0	4250	62.1
GF_{75min}	79.5	1449	96.3
GF_{90min}	66.5	653	124.7
GF_{120min}	39.3	158	190.5
GF_{S12}	—	92	198.1
GF_{S13}	—	63	201.4
1-Layer GF (Cu)[21]	97.4	272	5100
7-Layer GF (Cu)[23]	83.7	220	450.8
GF (SiO_2)[6]	80.0	4000	—
	90.0	20000	—
GF (Reduced-GO)[22]	80.0	8000	—
420 nm-FTO[20]	84.1	15.0	20.0

[a] Note: GF_{30min}, GF_{60min}, GF_{75min}, GF_{90min}, GF_{120min}, GF_{S12} and GF_{S13} are the graphene films prepared by APCVD for samples S6, S8, S9, S10, S11, S12 and S13. GF (Cu), GF (SiO_2) and GF (reduced-GO) are defined as the graphene films grown on Cu and SiO_2 substrates, and annealed on SiO_2 substrates from self-assembled graphene oxide (GO).

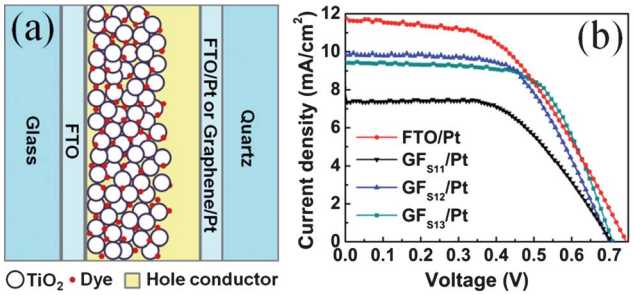

Fig. 7 (a) Schematic diagram and (b) *J–V* characteristics of the dye-sensitized solar cells based on FTO/Pt and graphene/Pt counter electrodes. GF_{S11}, GF_{S12} and GF_{S13} are defined as the graphene films for samples S11, S12 and S13 described in the ESI.†

of the substitution of expensive FTO, which is widely used as a counter electrode in DSSCs.[23,24] The photocurrent density–voltage (*J–V*) characteristics of the graphene-containing devices are shown in Fig. 7b. The DSSC, based on the graphene film with a sheet resistance of 158 Ω sq^{-1} and a mobility of 190.5 $cm^2\ v^{-1}\ s^{-1}$, shows a short-circuit photocurrent density (J_{sc}) of 7.4 mA cm^{-2}, an open-circuit voltage (V_{oc}) of 0.71 V, a fill factor (FF) of 56.4%, and an overall PCE of 2.9%. This demonstrates that the graphene film can be used as the counter electrode in DSSCs. To further optimize the cell efficiency, the graphene films for samples S12 and S13 with more excellent electrical properties are used as counter electrodes, and their efficiencies reach up to 4.00% and 4.25%, respectively. The best efficiency (V_{oc} = 0.71 V, J_{sc} = 9.45 mA cm^{-2}, FF = 63.5%, $\eta = 4.25\%$) is quite close to that using a Pt/FTO counter electrode (4.32%), as listed in Table 2, suggesting the graphene films are very promising counter electrodes for DSSCs.

Apparently, although the J_{sc} of graphene-containing DSSCs is lower than those using FTO, such a high efficiency is mainly attributed to the significant improvement in the FF from 49.8% to 63.5%. This is because the graphene films directly grown on SiO_2 substrates exhibit a relatively low sheet resistance (~63.0 Ω sq^{-1}). More importantly, the graphene films also supply an extremely high mobility (~201.4 $cm^2\ v^{-1}\ s^{-1}$), which is conducive to separate carriers (holes/electrons) and allows light-induced carriers to be more promptly collected. In addition, the surface of graphene films is not smooth, and many graphene sheets can form a 3D porous network structure, which can supply a large surface area for the support of Pt nanoparticles as much as possible. The unusual 3D network of graphene films is responsible for the high electrochemical activity of graphene counter electrodes, resulting in the excellent PV performance of DSSCs. On the other hand, the efficiency of graphene based DSSCs can be improved further by optimizing electrical properties of graphene films and device architectures in the future.

Table 2 Sheet resistance (R_s), electron mobility (μ) and photovoltaic performance comparisons of FTO/Pt and graphene/Pt counter electrodes in DSSCs

Counter Electrode	R_s (Ωsq^{-1})	μ ($cm^2\ v^{-1}\ s^{-1}$)	J_{sc} (mA cm^{-2})	V_{oc} (V)	FF (%)	η (%)
FTO/Pt	15.0	20.0	11.68	0.74	49.8	4.32
GF_{S11}/Pt	158.0	190.5	7.34	0.71	56.8	2.95
GF_{S12}/Pt	92.0	198.1	9.88	0.71	57.1	4.00
GF_{S13}/Pt	63.0	201.4	9.45	0.71	63.5	4.25

4. Conclusions

In summary, we have developed a new growth approach for the direct deposition of graphene films on SiO_2 substrates by APCVD, and the graphene films have been successfully incorporated in DSSCs as counter electrodes. The layer number and in-plane crystal size of the graphene films can be controlled by varying the growth conditions. High growth temperature, long growth time and large flow rate ratios of CH_4 to H_2 are beneficial to obtain thicker and larger graphene sheets for the formation of continuous graphene films on SiO_2 substrates. Moreover, nearly the same quality graphene films can also grow on BN, SiO_2/Si, AlN and Si substrates. The graphene films directly grown on SiO_2 substrates exhibit outstanding photoelectric properties, having a transparency from 98.1% (30 min growth) to 39.9% (120 min growth) at 550 nm, and the respective sheet resistances vary from 16540 Ω sq^{-1} to 158 Ω sq^{-1}. In addition, the graphene films with a sheet resistance of ~63.0 Ω sq^{-1} and an electron mobility of ~201.4 $cm^2\ v^{-1}\ s^{-1}$ can be obtained by further increasing the growth time and the flow rate of CH_4, and the graphene films are used as counter electrodes to fabricate prototype devices with a SiO_2/graphene–Pt/electrolyte/dye-sensitized TiO_2/FTO/glass configuration. The best photovoltaic efficiency reaches up to 4.25%, quite close to the performance (4.32%) of FTO electrode devices, providing encouraging evidence that the highly conductive graphene films may be used as new low cost electrode materials for thin film photovoltaic devices.

Acknowledgements

Financial supports from National 973 & 863 Program of China Grant No. 2009CB939903 & 2011AA050505, National Science Fund for Distinguished Young Scholars of China Grant No. 51125006, NSF of China Grant No. 50821004 & 61106088 & 50902143 & 21101164 & 61076062 & 51102263 & 91122034, Science and Technology Commission of Shanghai Grant No. 10520706700 & 10JC1415800, National Science and Technology Major Project Grant No. 2011ZX02707, China Postdoctoral Science Foundation Grant No. 20100480632 and Shanghai Postdoctoral Science Foundation Grant No. 11R21416900 are acknowledged.

Notes and references

1 R. R. Nair, P. Blake, A. N. Grigorenko, K. S. Novoselov, T. J. Booth, T. Stauber, N. M. R. Peres and A. K. Geim, *Science*, 2008, **320**, 1308.
2 H. Bi, F. Q. Huang, J. Liang, Y. F. Tang, X. J. Lü, X. M. Xie and M. H. Jiang, *J. Mater. Chem.*, 2011, **21**, 17366.
3 K. S. Kim, Y. Zhao, H. Jang, S. Y. Lee, J. M. Kim, K. S. Kim, J. H. Ahn, P. Kim, J. Y. Choi and B. H. Hong, *Nature*, 2009, **457**, 706–710.
4 X. Li, W. Cai, J. An, S. Kim, J. Nah, D. Yang, R. Piner, A. Velamakanni, I. Jung, E. Tutuc, S. K. Banerjee, L. Colombo and R. S. Ruoff, *Science*, 2009, **324**, 1312–1314.
5 S. K. Jerng, D. S. Yu, Y. S. Kim, J. Ryou, S. Hong, C. Kim, S. Yoon, D. K. Efetov, P. Kim and S. H. Chun, *J. Phys. Chem. C*, 2011, **115**, 4491–4494.

6 K. B. Kim, C. M. Lee and J. Choi, *J. Phys. Chem. C*, 2011, **115**, 14488–14493.
7 C. M. Lee and J. Choi, *Appl. Phys. Lett.*, 2011, **98**, 183106.
8 L. Zhang, Z. Shi, Y. Wang, R. Yang, D. Shi and G. Zhang, *Nano Res.*, 2011, **4**, 315–321.
9 X. Ding, G. Ding, X. Xie, F. Huang and M. Jiang, *Carbon*, 2011, **49**, 2522–2525.
10 M. H. Rümmeli, A. Bachmatiuk, A. Scott, F. Borrnert, J. H. Warner, V. Hoffman, J. H. Lin, G. Cuniberti and B. Büchner, *ACS Nano*, 2010, **4**, 4206–4210.
11 Y. Wang, S. W. Tong, X. F. Xu, B. Özyilmaz and K. P. Loh, *Adv. Mater.*, 2011, **23**, 1514–1518.
12 X. Li, H. Zhu, K. Wang, A. Cao, J. Wei, C. Li, Y. Jia, Z. Li, X. Li and D. Wu, *Adv. Mater.*, 2010, **22**, 2743–2748.
13 H. Bi, F. Q. Huang, J. Liang, X. M. Xie and M. H. Jiang, *Adv. Mater.*, 2011, **23**, 3202–3206.
14 A. C. Ferrari, J. C. Meyer, V. Scardaci, C. Casiraghi, M. Lazzeri, F. Mauri, S. Piscanec, D. Jiang, K. S. Novoselov, S. Roth and A. K. Geim, *Phys. Rev. Lett.*, 2006, **97**, 187401.
15 D. W. Zhang, X. D. Li, H. B. Li, S. Chen, Z. Sun, X. J. Yin and S. M. Huang, *Carbon*, 2011, **49**, 5382–5388.
16 D. H. Seo, S. Kumar and K. Ostrikov, *Carbon*, 2011, **49**, 4331–4339.
17 L. Cancado, K. Takai, T. Enoki, M. Endo, Y. Kim, H. Mizusaki, A. Jorio, L. Coelho, R. Magalhaes-Paniago and M. Pimenta, *Appl. Phys. Lett.*, 2006, **88**, 163106.
18 F. Kurdesau, G. Khripunov, A. F. da Cunha, M. Kaelin and A. N. Tiwari, *J. Non-Cryst. Solids*, 2006, **352**, 1466–1470.
19 C. Agashe, O. Kluth, J. Hüpkes, U. Zastrow, B. Rech and M. Wuttig, *J. Appl. Phys.*, 2004, **95**, 1911.
20 C. Agashe, J. Hüpkes, G. Schöpe and M. Berginski, *Sol. Energy Mater. Sol. Cells*, 2009, **93**, 1256–1262.
21 S. Bae, H. Kim, Y. Lee, X. Xu, J. S. Park, Y. Zheng, J. Balakrishnan, T. Lei, H. Ri Kim, Y. I. Song, Y. J. Kim, K. S. Kim, B. Ozyilmaz, J. H. Ahn, B. H. Hong and S. Iijima, *Nat. Nanotechnol.*, 2010, **5**, 574–578.
22 X. Li, G. Zhang, X. Bai, X. Sun, X. Wang, E. Wang and H. Dai, *Nat. Nanotechnol.*, 2008, **3**, 538–542.
23 X. Lü, X. Mou, J. Wu, D. Zhang, L. Zhang, F. Huang, F. Xu and S. Huang, *Adv. Funct. Mater.*, 2010, **20**, 509–515.
24 X. Lü, F. Huang, X. Mou, Y. Wang and F. Xu, *Adv. Mater.*, 2010, **22**, 3719–3722.

